AGU ADVANCING EARTH AND SPACE SCIENCES

Geophysical Research Letters

RESEARCH LETTER
10.1029/2023GL106166

A New Atmospheric Background State to Diagnose Local Waveguidability

Christopher Polster[1] and **Volkmar Wirth**[1]

[1]Institute for Atmospheric Physics, Johannes Gutenberg University, Mainz, Germany

Key Points:

- We construct a new atmospheric background state that is local in both space and time
- Waveguide information can be extracted from the background state potential vorticity field
- Our scheme enables instantaneous waveguide analysis while also reproducing established waveguide patterns after long-term aggregation

Correspondence to:
C. Polster,
cpolster@uni-mainz.de

Citation:
Polster, C., & Wirth, V. (2023). A new atmospheric background state to diagnose local waveguidability. *Geophysical Research Letters*, *50*, e2023GL106166. https://doi.org/10.1029/2023GL106166

Received 30 AUG 2023
Accepted 3 DEC 2023

Abstract A new procedure to obtain a longitudinally varying and slowly evolving atmospheric background state for the analysis of Rossby waveguides is described and discussed. The procedure is a rolling zonalization scheme, redistributing Ertel potential vorticity in a moving window to separate waves from the background. Waveguides are subsequently diagnosed from the gradient of the logarithm of potential vorticity. The effectiveness of the wave-background separation, even in large-amplitude conditions, is illustrated with reanalysis data. Established climatological-mean waveguide structures are recovered from the rolling-zonalized state in the limit of long-term aggregation. Two contrasting episodes of Rossby wave packet propagation demonstrate how the evolution of waveguides derived from rolling zonalization can correspond to the development of superposed wave packets. The ability of the procedure to work with snapshots of the atmosphere provides new opportunities for waveguide research.

Plain Language Summary Rossby waves are meridional excursions of the jet stream, a strong band of wind in the extratropics. Stationary Rossby waves can cause extreme weather at the surface and traveling waves connect the weather of remote regions on the globe. Paths along which Rossby waves preferentially develop and travel are called waveguides. To detect the presence of a waveguide in atmospheric data, the waves have to be separated from their guiding atmospheric background state first. We introduce a new separation procedure for snapshots of the atmosphere that results in a slowly evolving and longitudinally varying background state. Our background state is a new source of local waveguide information, particularly in applications where no reliable information was available previously.

1. Introduction

Waveguides are paths in the atmosphere along which Rossby wave activity is preferentially ducted (Branstator, 1983; Chang & Yu, 1999; Hoskins & Ambrizzi, 1993; Martius et al., 2010; Wirth et al., 2018). The concept of a waveguide is important for understanding teleconnection patterns facilitated by Rossby waves (Branstator, 2002; Branstator & Teng, 2017; Hoskins & Karoly, 1981; Hsu & Lin, 1992), the steering of weather systems (Chang et al., 2002), the onset of atmospheric blocking (Nakamura & Huang, 2018), extreme weather (Kornhuber et al., 2017; Petoukhov et al., 2013; Rousi et al., 2022; White et al., 2022) and sub-seasonal to seasonal weather prediction (Davies, 2015; Hoskins, 2013). In this work, we focus on the horizontal propagation of Rossby waves along the extratropical jet waveguide.

Strong and narrow jet streams are known to constitute good Rossby waveguides in the atmosphere (Harvey et al., 2016; Manola et al., 2013; Wirth, 2020). In practice, jet detection schemes (e.g., Koch et al., 2006; Spensberger et al., 2017) and jet-associated enhanced gradients of potential vorticity (e.g., Martius et al., 2010; Massacand & Davies, 2001; Röthlisberger et al., 2016; Schwierz et al., 2004) are used to extract waveguide information from atmospheric data. Waveguides are diagnosed in barotropic analysis by tracing Rossby waves as rays refracted by the stationary wavenumber field (Ambrizzi et al., 1995; Hoskins & Ambrizzi, 1993; Karoly, 1983), though concerns about the underlying assumptions of the theory have been raised since its inception (Hoskins & Karoly, 1981; Teng & Branstator, 2019; Wirth, 2020). Figure 1 illustrates the general agreement of common diagnostic fields regarding the mean climatological waveguide patterns.

The conceptual picture considers waveguides as features of a wave-free background state onto which waves are superposed. Separating waves and background in the atmosphere post factum is a challenging and not well defined problem, as the scale of both can overlap in time and space (Branstator & Teng, 2017; Wirth & Polster, 2021). Temporal and spatial filters are nevertheless often applied in practice, supported, for example, by the finding that waveguides diagnosed from long-term means reflect the known large-scale teleconnection patterns and storm

10.1029/2023GL106166

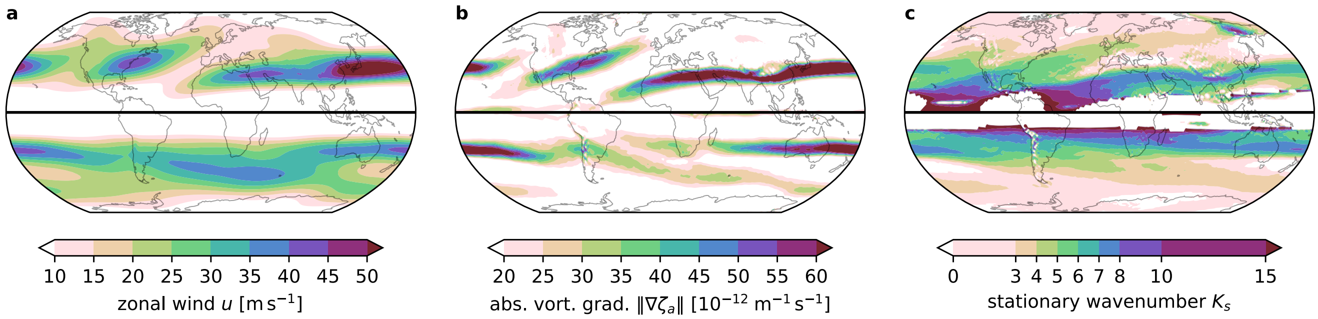

Figure 1. Barotropic waveguide diagnostic fields computed from the 1979–2022 ERA5 winter-mean horizontal wind fields on the 330 K isentrope. (a) Zonal wind component u. (b) Magnitude of the gradient of absolute vorticity ζ_a. (c) Stationary zonal wavenumber K_s, with $K_s^2 = a\,\cos(\phi)^2 u^{-1} \partial_\phi \zeta_a$ (see text for symbols) and imaginary values plotted white. In general, Rossby waves are expected to propagate preferentially along maxima of these fields. Both hemispheres show winter, that is, DJF on the northern and JJA on the southern hemisphere.

track regions (Figure 1). However, closer examination reveals representativity issues due to approximations such as zonally symmetric background states (Borges & Sardeshmukh, 1995; Branstator, 1983, 2002; Hoskins & Ambrizzi, 1993) and internal variability (Spensberger et al., 2017) and the possibility of artifacts introduced by inadequate wave-background separation (Dritschel & Scott, 2011; Wirth & Polster, 2021). A separation scheme local in both time and space and resistant to producing artifacts in large-amplitude conditions has not been established so far.

The objective of the present work is to introduce a localized zonalization scheme as a novel method to compute a background state from a snapshot of the atmosphere for the purpose of waveguide analysis. Our scheme is both an extension and approximation of the computation of the modified Lagrangian mean state of Nakamura and Solomon (2011) and Methven and Berrisford (2015), adding longitudinal variability by means of a rolling window. Section 2 elaborates on the construction of our procedure and the used waveguide diagnostic. A background state is then computed from a reanalysis data set (Section 3) and evaluated regarding its use as a basis for waveguide analysis in Section 4. We conclude with a summary and discussion in Section 5.

2. Methods

2.1. Zonalization

Zonalization is a conservative rearrangement of potential vorticity (PV), such that the values of the resulting zonally symmetric PV profile are in descending order from North to South (Nakamura & Zhu, 2010). We zonalize Ertel PV, in isentropic coordinates given by $q = \frac{\zeta_a}{\sigma}$, the quotient of absolute vorticity ζ_a and isentropic density $\sigma = -\frac{1}{g}\frac{\partial p}{\partial \theta}$, with potential temperature θ, pressure p and gravitational acceleration g. The equivalent latitude ϕ_{eq} of a given PV contour of value Q (Allen & Nakamura, 2003; Butchart & Remsberg, 1986; Nakamura & Solomon, 2011) is implicitly defined as

$$\int_{q \geq Q} \sigma \, \mathrm{d}S = \int_{\phi \geq \phi_{\mathrm{eq}}} \sigma_{\mathrm{ref}} \, \mathrm{d}S, \tag{1}$$

where both integrals are surface integrals evaluated on an isentrope and ϕ is latitude. The integrals evaluate to the layer mass (in kg K^{-1}) enclosed by the contour Q or latitude ϕ_{eq}, respectively. The background-state isentropic density σ_{ref} must be prescribed for the computation. In this work, we evaluate relation Equation 1 in a rolling fashion along longitude, using a 60°-wide window, to obtain a longitudinally varying zonalized state. The zonalized PV profile is determined for every window position and assigned to the central longitude of the window (Figure 2b). We call this procedure rolling zonalization and the resulting field of zonalized PV profiles (Figure 2d) a rolling-zonalized background state.

Rolling zonalization can be adjusted to the needs of different applications by selecting different window widths, but the choice of this parameter also introduces subjectivity. For the purpose of waveguide detection, we have found results to be robust in the range of window widths from 60° to 90° and have chosen 60° as our default here. To be sure, the addition of longitudinal variation invalidates many theoretical results derived for the hemispherically

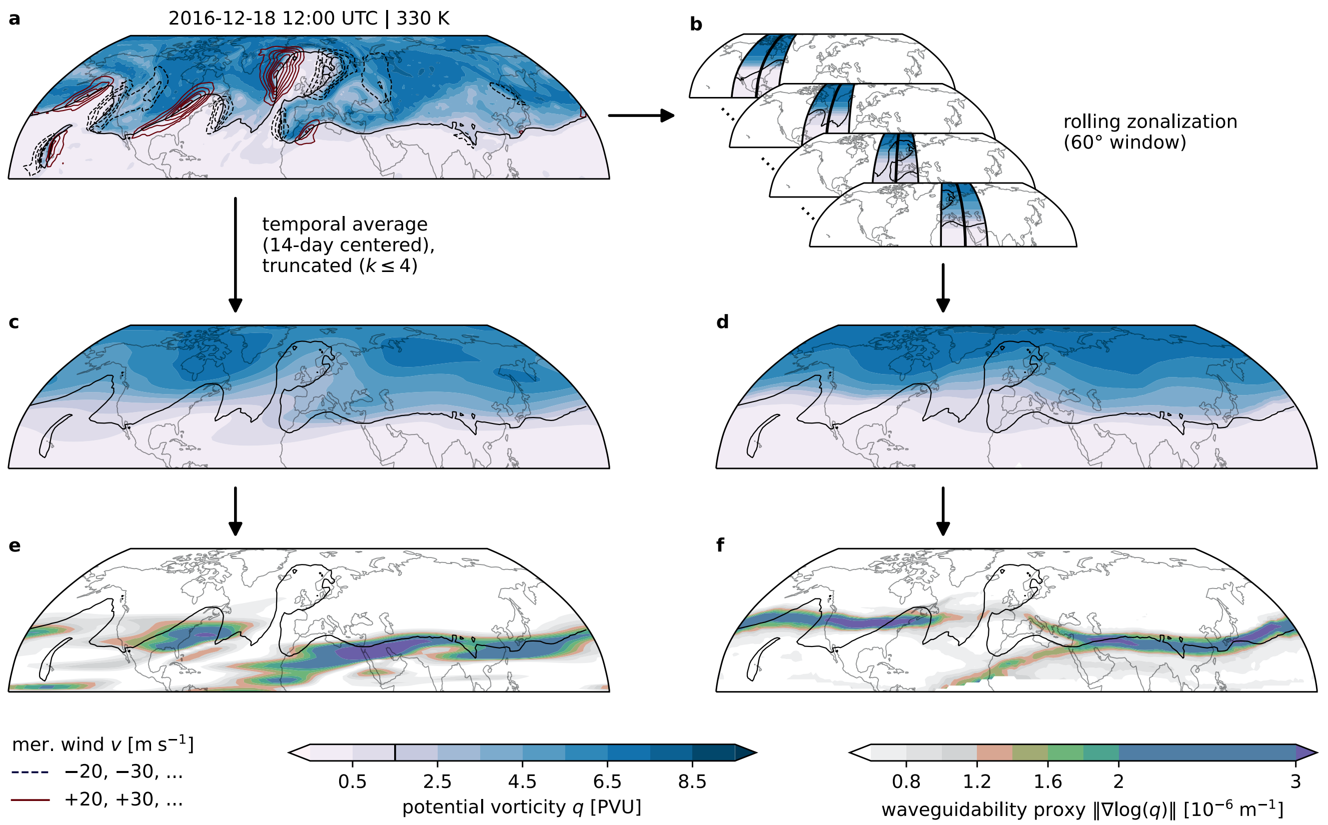

Figure 2. Comparison of time-mean and rolling-zonalized background states on the 330 K isentrope. (a) PV (filled contours) and meridional wind (red and black dashed contours) on 18 December 2016 1200 UTC. For convenience, the 1.5 PVU contour of PV is shown in all panels (solid black). (b) Rolling zonalization illustrated by four individual zonalizations for 90°W, 50°W, 10°W, and 30°E. Each window's central longitude is highlighted in bold. (c) 14 days-mean PV after application of a zonal wavenumber filter (truncation after wavenumber 4). (d) Rolling-zonalized PV. (e,f) $\|\nabla \log(q)\|$ as a waveguide diagnostic, based on (c, d), respectively.

zonalized state (Nakamura & Solomon, 2011; Methven & Berrisford, 2015; Ghinassi et al., 2020). We do not attempt to recover localized versions of these theorems in this work, but note that the localized zonalized state can be changed both by non-conservative processes (diabatic, frictional or mixing, as for the hemispherically zonalized state; Methven & Berrisford, 2015) and by zonal rearrangement of PV. These processes can lead to significant local changes in the background state, for example, during episodes of atmospheric blocking which are often associated with horizontal PV advection (Hauser et al., 2023; H. Nakamura et al., 1997), cross-isentropic PV transport due to latent heat release (Pfahl et al., 2015; Steinfeld et al., 2020) and irreversible mixing of PV during wave breaking (Berrisford et al., 2007; Masato et al., 2012).

The process of applying zonalization in a rolling fashion does not guarantee that PV is globally conserved, even though each individual zonalization is conservative. The loss of exact PV conservation is one of multiple approximations made to facilitate a simple and practical implementation of our procedure. A significant departure from the ELIPVI zonalization scheme of Methven and Berrisford (2015) is the omission of PV inversion and an iteration to a consistent background isentropic density field. Instead, we prescribe σ_{ref} based on a longitudinally rolling mean of σ using the same window width as the zonalization. The lack of PV inversion also means that other “byproducts” like the background state wind are not computed in our approximation. A three-dimensional hemispheric PV inversion required for a localized ELIPVI implementation presents a significant technical challenge. For practical reasons and accessibility we do not want to incur the substantial computational costs of an inversion-based procedure. By contrast, a rolling zonalization can be computed in about 100 ms on a single CPU core.

2.2. Waveguide Diagnostic

We diagnose waveguidability, a non-binary assessment of the propensity of the atmosphere to duct Rossby waves (Manola et al., 2013; Wirth, 2020), based on the gradient of the logarithm of the background state PV obtained from the rolling zonalization. An example of this field is shown in Figure 2f. To first order, $\|\nabla \log(q)\|$ is proportional to the curvature of the flow $\nabla^2 u$ and thus related to the dispersion relation of Rossby waves (Bukenberger et al., 2023; Martius et al., 2010). We aim to avoid issues associated with strong variations of stratification when deriving the location of waveguides from $\|\nabla \log(q)\|$ (Bukenberger et al., 2023) with the rolling mean-smoothed σ_{ref}. Regions where $|q| < 0.1$ PVU (1 PVU = 10^{-6} K m^2 kg^{-1} s^{-1}) are excluded in our waveguide analysis to avoid the divergence of the logarithm when $q \to 0$. As a simple criterion for the presence of a waveguide, we require $\|\nabla \log(|q|)\| > 1.2 \times 10^{-6}$ m^{-1}, with q in PVU. We have verified that our results are not sensitive to the choice of this threshold.

3. Data and Software

We process ERA5 (Hersbach et al., 2020, 2023) reanalysis fields of u, v, and T from 1979 to 2022 (6-hourly). The input fields are obtained with 1.5° horizontal resolution on 18 pressure levels (50–850 hPa in steps of 50 hPa; 70 hPa additionally). We compute potential temperature and isentropic density (clipping negative values at 0) on pressure levels, then interpolate to isentropes. Vorticity is computed from the interpolated winds and combined with the interpolated isentropic density to calculate PV. Surface integrals for the zonalization are evaluated for a set of automatically chosen PV contours $\{Q_1, Q_2, \ldots, Q_n\}$ with a conditional boxcounting quadrature scheme, and regions outside the input data range omitted. Zonalized PV profiles are interpolated from the equivalent latitudes back to the regular latitude grid for convenience. We zonalize each hemisphere separately. More details about our implementation of the rolling zonalization can be found in the documentation of our open-source software (Polster, 2023).

4. Results

4.1. A First Look

We take a first look at a rolling-zonalized state in Figure 2d. The selected date is from a European blocking event in December 2016 (Maddison et al., 2019; Polster & Wirth, 2023). The rolling-zonalized PV exhibits a wavenumber 2 to 3 pattern in the midlatitudes. The meridional spacing of background state PV contours widens locally over western Europe and resembles an often assumed background state configuration of scale interaction models of atmospheric blocking (Luo et al., 2023). The associated weakened gradient of PV is reflected in our waveguide diagnostic field (Figure 2f). With a threshold of 1.2×10^{-6} m^{-1}, we detect an interruption of the waveguide in the blocking region, while a strong and continuous waveguide is found over subtropical Asia and the midlatitude Pacific and North American regions. Interestingly, our scheme detects strong waveguidability over Asia despite no wave being present there.

Comparing the rolling-zonalized (Figure 2d) and the 14-day temporally averaged PV fields after truncation at wavenumber 4 (Figure 2c), we find some common features, but at the same time important differences in the details. The averaged and truncated PV field is also dominated by a wavenumber 2 to 3 structure. The meridional profile of PV is non-monotonic at many longitudes of Figure 2c and contour overturning at the block location indicates a failure of the temporal average-wavenumber filter to remove a stationary, large-amplitude eddy. The associated $\|\nabla \log(q)\|$ field (Figure 2e) features similar magnitudes as the rolling-zonalized state but structures are more blotchy. A waveguide interruption is also found at the block location but the waveguide across the hemisphere is generally less coherent compared to that in Figure 2f and zonally elongated artifacts from the wavenumber filtering are apparent, for example, along the west coast of Africa.

4.2. Filtering Properties

The temporal evolution of a hemispherically zonalized state is known to be inherently slow (Methven & Berrisford, 2015; Nakamura & Solomon, 2011). Figure 2 suggests that rolling zonalization can produce fields with a broadly similar structure compared to those produced by a temporal filter, despite only using instantaneous data. In an analysis of 44 years of 6-hourly rolling-zonalized PV based on autocorrelation and spectral decomposition we found that the rolling-zonalized background state also evolves inherently slowly, although the characteristics of the temporal behavior do not correspond directly to that of any temporal filter we compared against (not shown).

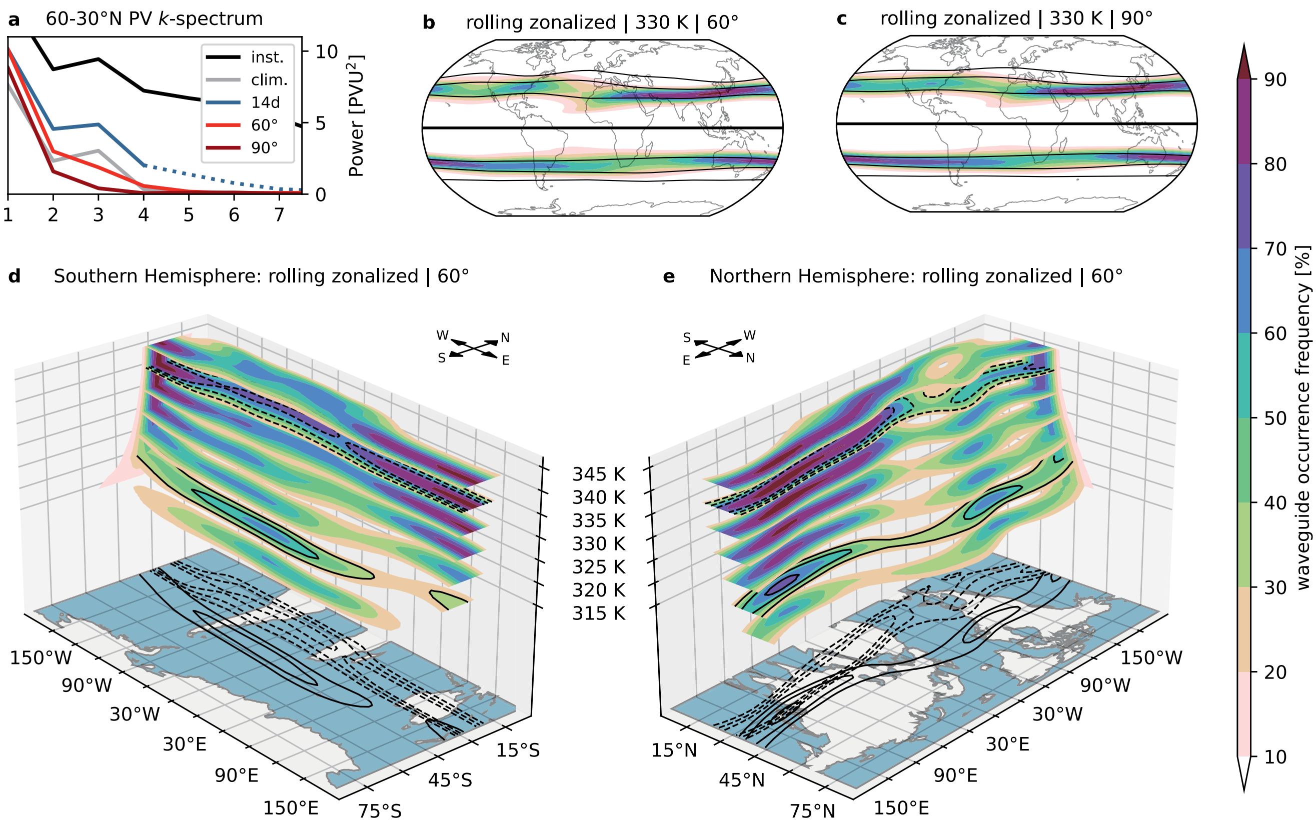

Figure 3. (a) Zonal Wavenumber spectra of instantaneous PV (black), climatological-mean PV (gray), 14 days-rolling-averaged PV (blue, dotted after the truncation threshold applied in Figure 2c) and 60°- (light red) and 90°-window (dark red) rolling-zonalized PV. All spectra of winter months only, spectral power averaged from 60 to 30°N on 330 K. (b, c) Climatological waveguide occurrence on 330 K during winter, derived from a rolling-zonalized state with a 1.2×10^{-6} m^{-1} waveguide detection threshold. Mean contours of rolling-zonalized PV are shown in black. Comparison of 60° (b) and 90° (c) window widths. (d,e) Waveguide occurrence as in (b) but for isentropic levels from 315 to 345 K in steps of 5 K in a 3D visualization for each hemisphere. Selected contours from the 320 (solid) and 340 K (dashed) isentropic levels are reproduced on the bottom maps for orientation. Note that the actual surface of the planet is not a surface of constant potential temperature as depicted here.

A rolling-zonalized state (60° window) cuts off virtually all contributions of waves with wavenumbers equal to or larger than 5 in the zonal wavenumber power spectrum of PV (Figure 3a). Wavenumbers 1, 2, and 3 contribute almost all spectral power in the Northern Hemisphere midlatitudes, with only minor contributions from wavenumber 4. We consider the rolling-zonalized state therefore to be free of synoptic- and smaller-scale eddies. Widening the window of the rolling zonalization to 90° reduces the power in wavenumbers 2 to 4 significantly and moves the cut-off wavelength to $k = 4$. By comparison, a 14-day rolling mean retains more overall spectral power than the rolling-zonalized states. There is still as much power in wavenumber 6 after temporal averaging than the 60° rolling-zonalized state has in wavenumber 4 so that an additional zonal wavenumber filter is required to remove smaller-scale features. In the spectral comparison of Figure 3a, the 60° rolling-zonalized state is closest to the climatological mean state. The spatial filtering properties of rolling zonalization are generally not unlike, but in details importantly different to those of simple averaging or spectral truncation procedures.

4.3. Climatological Waveguide Occurrence

Using the 1.2×10^{-6} m^{-1} threshold, we compute the gridpoint-wise occurrence frequency of waveguides in the rolling-zonalized state. Figure 3b shows the winter-time waveguide occurrence for our default window with of 60° longitude on 330 K. Frequent occurrence of an Asian subtropical waveguide extending into the Pacific and a North American/North Atlantic waveguide can be identified on the Northern Hemisphere. On the Southern Hemisphere, a band of more than 40% waveguide occurrence extends around the globe in the midlatitudes with waveguides occurring preferentially in the Pacific sector from Australia to South America. Figure 3c shows the same analysis for a 90°-wide window, resulting in more zonally elongated waveguide occurrence features.

AGU ADVANCING EARTH AND SPACE SCIENCES
Geophysical Research Letters
10.1029/2023GL106166

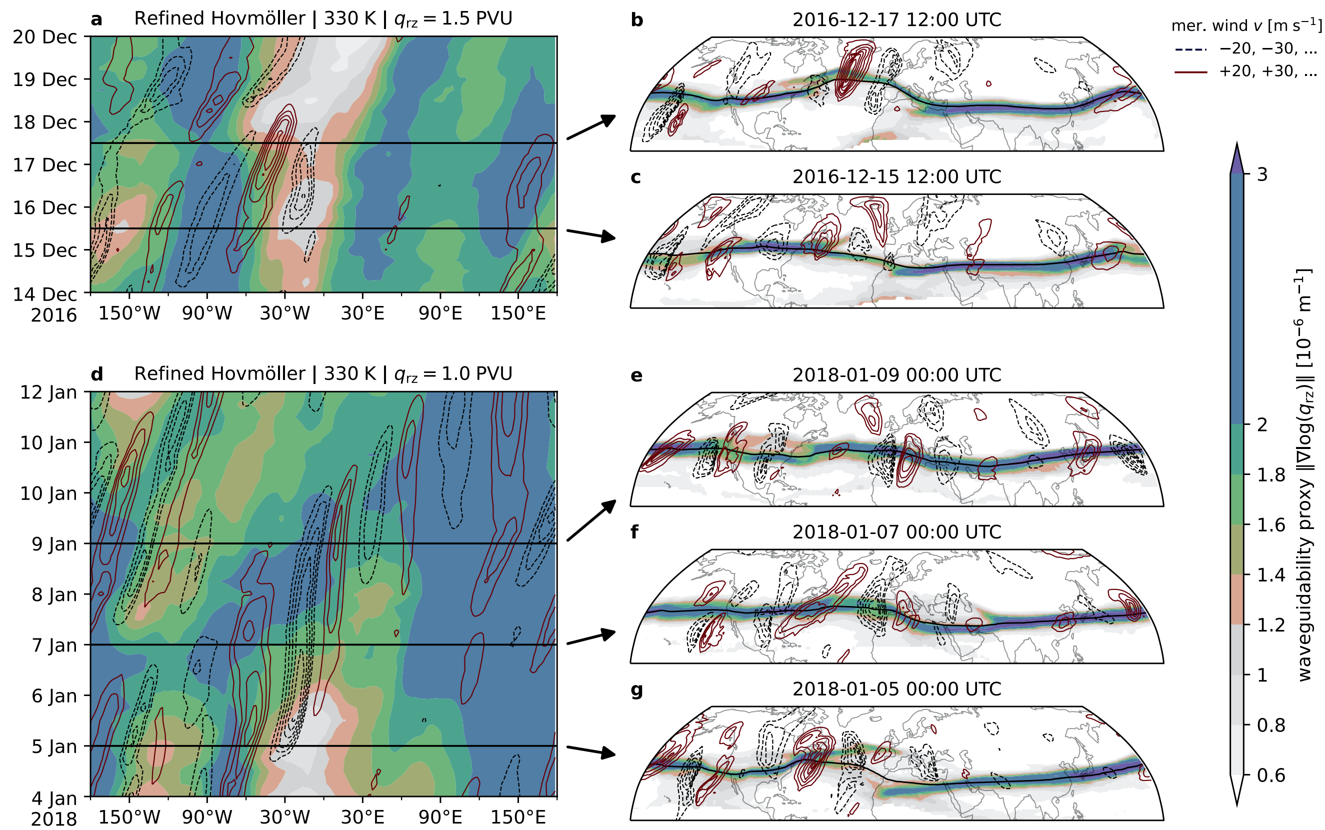

Figure 4. (a) Refined Hovmöller diagram of meridional wind (contours) and the grad-log-PV waveguide diagnostic (filled contours) applied to the rolling-zonalized background state (q_{rz}). Data is extracted with a 7.5° boxcar smoothing kernel along the 1.5 PVU contour. (b, c) $\|\nabla \log(q_{rz})\|$ waveguidability diagnostic (filled contours), 1.5 PVU contour of rolling-zonalized PV (black) and meridional wind (dark red/blue contours, in steps of 10 m s^{-1} starting from ±20 m s^{-1}) on 330 K for 17 and 15 December 2016 1200 UTC, respectively. (d) Like (a), but for 4–12 December 2018 and along 1 PVU. (e–g) Like (b), but for 9, 7, and 5 December 2018, respectively, and a PV contour of 1 PVU.

The identity of the North Atlantic waveguide as a feature separate from the North Pacific waveguide is less pronounced but differences between the window widths are otherwise small.

We compare the climatological mean barotropic waveguide diagnostic fields in Figure 1 with the waveguide occurrence frequency field in Figure 3b. The climatological mean winter waveguide structure is broadly reproduced in the long-term aggregated waveguide information from individual snapshots of the rolling-zonalized atmosphere. Relative signal strengths of co-located features in Figures 1 and 3b are similar. However, the waveguide signal associated with the North Atlantic jet does not extend as far toward Europe in the frequency field of the rolling-zonalized state and a secondary waveguide over the Atlantic and Indian Ocean on the Southern Hemisphere is missing. Differences in the waveguide features can be contextualized with the vertical structure of waveguide occurrence in Figures 3d and 3e. The vertical structure shows the distinct identities of the North Atlantic and Asian/Pacific waveguides on the Northern Hemisphere more clearly than 330 K alone. The midlatitude waveguides over the North and South Atlantic oceans are primarily found on lower isentropic levels than 330 K, while the subtropical waveguides are found at higher levels (Martin, 2021; Martius et al., 2010).

4.4. Two Contrasting Episodes

We use a refined Hovmöller diagram (Martius et al., 2006) to further illuminate the waveguide evolution around the December 2016 blocking episode introduced in Section 4.1 and Figure 2. Note that the generation of such contour-following Hovmöller diagrams is particularly easy in the rolling-zonalized state as each PV contour intersects a meridian at most once by construction. Figure 4a shows the evolution of $\|\nabla \log(q)\|$, our waveguidability metric, along the 1.5 PVU contour on 330 K for the 2016 episode. In the snapshot for 15 December (Figure 4c), a Rossby wave packet (RWP) stretches from North America across the North Atlantic into northern

Europe, superposed onto a strong waveguide over North America. The waveguide is weaker over the Atlantic with a connection to the subtropical waveguide over Asia and a second short branch pointing toward northern Europe. Over the next 2 days the waveguide strengthens over the Atlantic while shifting northward together with the 1.5 PVU contour (Figure 4b). A day later, the waveguide is interrupted (cf. Figure 2f) and the propagation of the RWP ceases as the block has been established (Polster & Wirth, 2023), with low waveguidability dominating the sector after 17 December (Figure 4a).

A different evolution of waveguide and wave is seen in an episode from January 2018 (Figures 4d–4g). On 5 January (Figure 4g), a North Atlantic waveguide ends about 20° further north than a subtropical waveguide over Africa starts, with no significant connection between both. A Rossby wave packet stretches across the Atlantic along the waveguide. Strong meridional winds develop over the North Atlantic but the wave packet does not propagate through the African/European region at first. During 6 January, the two waveguides connect over the Mediterranean (Figures 4d,f) and a wave signal emerges in the subtropics at the same time. By 9 January, a strong waveguide has been established from the North Atlantic across Asia to the North Pacific (Figure 4e). The evolution of the wave packet appears to occur along this waveguide, with new meridional wind extrema developing over the Arabian Peninsula and further downstream in the following days (Figure 4d).

The two episodes exhibit opposite RWP propagation characteristics in the African/European region. While the incoming RWP in December 2016 develops into a block with no downstream development over Asia, the wave packet in January 2018 continues development along the subtropical waveguide (akin to the equatorward wave energy transfer described by Martius et al., 2010). The parallel evolutions of the midlatitude and subtropical waveguides in these two episodes reflect these (non-)propagation patterns: the waveguides are effectively disconnected during the 2016 episode, while the waveguides connect in 2018.

5. Summary and Discussion

We have introduced a new procedure, rolling zonalization, to compute a three-dimensional background state of the atmosphere that evolves with time. The procedure consists of a rearrangement of potential vorticity in a longitudinally rolling sector on a hemisphere, based on the concept of equivalent latitude (Equation 1, Allen & Nakamura, 2003; Nakamura & Solomon, 2011; Methven & Berrisford, 2015; Wirth & Polster, 2021). Rolling zonalization combines aspects of both a spatial and a temporal filter. Synoptic-scale eddies of arbitrary amplitude are eliminated effectively by the zonalization. The resulting background state is slowly evolving even though no information other than the instantaneous state of the atmosphere is required to compute it.

Localizing zonalization with a rolling window is straightforward, but it is only an approximation of a scheme consistent with the underlying formalism. We do not compute consistent background fields of isentropic density or wind and strict PV conservation is not guaranteed, although we have observed good PV conservation for our setup. We leave the formulation of a theory of wave-mean flow interaction that accomodates our localized zonalized background state to future work. Our present objective is to advance the state of practical application.

Using the log-PV gradient of the rolling-zonalized background state as a waveguide diagnostic (Bukenberger et al., 2023; Martius et al., 2010; Schwierz et al., 2004), we were able to recover the established structure of the winter-time climatological waveguides in the extratropics (e.g., Ambrizzi et al., 1995; Hoskins & Ambrizzi, 1993). The aggregation of instantaneous waveguide information into a frequency-based perspective on waveguide occurrence complements earlier climatological mean-based results (see also White, 2019). Two contrasting episodes of Rossby wave packet propagation demonstrated how the zonalization-derived waveguides can correspond to the local development of superposed wave trains. An interrupted waveguide in the first episode coincided with the onset of a block. A connected waveguide in the second episode coincided with a transfer of wave activity from the midlatitude to the subtropical waveguide.

We can envisage further fine-tuning of the rolling zonalization procedure and waveguide diagnostics. Instead of a threshold-based binary view of waveguide occurrence, more nuanced information on waveguidabililty should be extractable from the background state. Our climatological waveguide analysis in isentropic coordinates highlighted the importance of vertical structure, but the implications for both horizontal and vertical (e.g., Nathan & Hodyss, 2010) propagation of Rossby waves remain unexplored here. Local wave activity (Ghinassi et al., 2018; Huang & Nakamura, 2016, 2017), computed with respect to the longitudinally varying zonalized background state, presents a more consistent measure of local waviness than the meridional wind. We intend to explore the relationship between waveguidability properties of the rolling-zonalized background state and wave packet propagation further in the future.

An atmospheric background state which is local in time and space and which is computable from instantaneous data enables diagnostics to be applied in the full range of lead times in forecast applications. Individual events can be investigated with regard to the influence of teleconnection patterns or the potential of resonance along a circumglobal waveguide. These are new and sought-after possibilities for current waveguidability research (e.g., Riboldi et al., 2022; White et al., 2022).

Data Availability Statement

The code to reproduce the data analysis and all figures of this article is preserved online (Polster, 2023). Procedures to compute the rolling zonalization are provided in a Python package included in the code repository. ERA5 data (Hersbach et al., 2023) was downloaded from the Copernicus Climate Change Service (C3S) Climate Data Store. The results contain modified Copernicus Climate Change Service information 2023. Neither the European Commission nor ECMWF is responsible for any use that may be made of the Copernicus information or data it contains.

Acknowledgments
We thank M. Riemer for valuable discussions about the rolling zonalization and its applications and acknowledge insightful conversations about the log-PV gradient waveguide diagnostic with M. Bukenberger and S. Schemm. Further thanks go to S. Schemm and an anonymous reviewer for their constructive comments on our manuscript during the review process. The research leading to these results has been carried out within the Transregional Collaborative Research Center SFB/TRR 165 "Waves to Weather" funded by the German Science Foundation (DFG).

References

Allen, D. R., & Nakamura, N. (2003). Tracer equivalent latitude: A diagnostic tool for isentropic transport studies. *Journal of the Atmospheric Sciences*, *60*(2), 287–304. https://doi.org/10.1175/1520-0469(2003)060⟨0287:TELADT⟩2.0.CO;2

Ambrizzi, T., Hoskins, B. J., & Hsu, H.-H. (1995). Rossby wave propagation and teleconnection patterns in the austral winter. *Journal of the Atmospheric Sciences*, *52*(21), 3661–3672. https://doi.org/10.1175/1520-0469(1995)052⟨3661:RWPATP⟩2.0.CO;2

Berrisford, P., Hoskins, B. J., & Tyrlis, E. (2007). Blocking and Rossby wave breaking on the dynamical tropopause in the Southern Hemisphere. *Journal of the Atmospheric Sciences*, *64*(8), 2881–2898. https://doi.org/10.1175/JAS3984.1

Borges, M. D., & Sardeshmukh, P. D. (1995). Barotropic Rossby wave dynamics of zonally varying upper-level flows during northern winter. *Journal of the Atmospheric Sciences*, *52*(21), 3779–3796. https://doi.org/10.1175/1520-0469(1995)052⟨3779:BRWDOZ⟩2.0.CO;2

Branstator, G. (1983). Horizontal energy propagation in a Barotropic atmosphere with meridional and zonal structure. *Journal of the Atmospheric Sciences*, *40*(7), 1689–1708. https://doi.org/10.1175/1520-0469(1983)040⟨1689:HEPIAB⟩2.0.CO;2

Branstator, G. (2002). Circumglobal teleconnections, the jet stream waveguide, and the North Atlantic Oscillation. *Journal of Climate*, *15*(14), 1893–1910. (Publisher: American Meteorological Society). https://doi.org/10.1175/1520-0442(2002)015⟨1893:CTTJSW⟩2.0.CO;2

Branstator, G., & Teng, H. (2017). Tropospheric waveguide teleconnections and their seasonality. *Journal of the Atmospheric Sciences*, *74*(5), 1513–1532. https://doi.org/10.1175/JAS-D-16-0305.1

Bukenberger, M., Rüdisühli, S., & Schemm, S. (2023). Jet stream dynamics from a PV gradient perspective: The method and its application to a km-scale simulation. *Quarterly Journal of the Royal Meteorological Society*, *149*(755), 2409–2432. https://doi.org/10.1002/qj.4513

Butchart, N., & Remsberg, E. E. (1986). The area of the stratospheric polar vortex as a diagnostic for tracer transport on an isentropic surface. *Journal of the Atmospheric Sciences*, *43*(13), 1319–1339. https://doi.org/10.1175/1520-0469(1986)043⟨1319:TAOTSP⟩2.0.CO;2

Chang, E. K. M., Lee, S., & Swanson, K. L. (2002). Storm track dynamics. *Journal of Climate*, *15*(16), 2163–2183. https://doi.org/10.1175/1520-0442(2002)015⟨02163:STD⟩2.0.CO;2

Chang, E. K. M., & Yu, D. B. (1999). Characteristics of wave packets in the upper troposphere. Part I: Northern Hemisphere winter. *Journal of the Atmospheric Sciences*, *56*(11), 1708–1728. https://doi.org/10.1175/1520-0469(1999)056⟨1708:COWPIT⟩2.0.CO;2

Davies, H. C. (2015). Weather chains during the 2013/2014 winter and their significance for seasonal prediction. *Nature Geoscience*, *8*(11), 833–837. https://doi.org/10.1038/ngeo2561

Dritschel, D. G., & Scott, R. K. (2011). Jet sharpening by turbulent mixing. *Philosophical Transactions of the Royal Society A: Mathematical, Physical & Engineering Sciences*, *369*(1937), 754–770. https://doi.org/10.1098/rsta.2010.0306

Ghinassi, P., Baumgart, M., Teubler, F., Riemer, M., & Wirth, V. (2020). A budget equation for the amplitude of Rossby wave packets based on finite-amplitude local wave activity. *Journal of the Atmospheric Sciences*, *77*(1), 277–296. https://doi.org/10.1175/JAS-D-19-0149.1

Ghinassi, P., Fragkoulidis, G., & Wirth, V. (2018). Local finite-amplitude wave activity as a diagnostic for Rossby wave packets. *Monthly Weather Review*, *146*(12), 4099–4114. https://doi.org/10.1175/MWR-D-18-0068.1

Harvey, B. J., Methven, J., & Ambaum, M. H. P. (2016). Rossby wave propagation on potential vorticity fronts with finite width. *Journal of Fluid Mechanics*, *794*, 775–797. https://doi.org/10.1017/jfm.2016.180

Hauser, S., Teubler, F., Riemer, M., Knippertz, P., & Grams, C. M. (2023). Towards a holistic understanding of blocked regime dynamics through a combination of complementary diagnostic perspectives. *Weather and Climate Dynamics*, *4*(2), 399–425. https://doi.org/10.5194/wcd-4-399-2023

Hersbach, H., Bell, B., Berrisford, P., Biavati, G., Horányi, A., Muñoz Sabater, J., et al. (2023). ERA5 hourly data on pressure levels from 1940 to present. *Copernicus Climate Change Service (C3S) Climate Data Store (CDS)*. https://doi.org/10.24381/cds.bd0915c6

Hersbach, H., Bell, B., Berrisford, P., Hirahara, S., Horányi, A., Muñoz-Sabater, J., et al. (2020). The ERA5 global reanalysis. *Quarterly Journal of the Royal Meteorological Society*, *146*(730), 1999–2049. https://doi.org/10.1002/qj.3803

Hoskins, B. J. (2013). The potential for skill across the range of the seamless weather-climate prediction problem: A stimulus for our science. *Quarterly Journal of the Royal Meteorological Society*, *139*(672), 573–584. https://doi.org/10.1002/qj.1991

Hoskins, B. J., & Ambrizzi, T. (1993). Rossby wave propagation on a realistic longitudinally varying flow. *Journal of the Atmospheric Sciences*, *50*(12), 1661–1671. https://doi.org/10.1175/1520-0469(1993)050⟨1661:RWPOAR⟩2.0.CO;2

Hoskins, B. J., & Karoly, D. J. (1981). The steady linear response of a spherical atmosphere to thermal and orographic forcing. *Journal of the Atmospheric Sciences*, *38*(6), 1179–1196. https://doi.org/10.1175/1520-0469(1981)038⟨1179:TSLROA⟩2.0.CO;2

Hsu, H.-H., & Lin, S.-H. (1992). Global teleconnections in the 250-mb streamfunction field during the Northern Hemisphere winter. *Monthly Weather Review*, *120*(7), 1169–1190. https://doi.org/10.1175/1520-0493(1992)120⟨1169:GTITMS⟩2.0.CO;2

Huang, C. S. Y., & Nakamura, N. (2016). Local finite-amplitude wave activity as a diagnostic of anomalous weather events. *Journal of the Atmospheric Sciences*, *73*(1), 211–229. https://doi.org/10.1175/JAS-D-15-0194.1

Huang, C. S. Y., & Nakamura, N. (2017). Local wave activity budgets of the wintertime Northern Hemisphere: Implication for the Pacific and Atlantic storm tracks. *Geophysical Research Letters*, *44*(11), 5673–5682. https://doi.org/10.1002/2017GL073760

Karoly, D. J. (1983). Rossby wave propagation in a barotropic atmosphere. *Dynamics of Atmospheres and Oceans*, *7*(2), 111–125. https://doi.org/10.1016/0377-0265(83)90013-1

Koch, P., Wernli, H., & Davies, H. C. (2006). An event-based jet-stream climatology and typology. *International Journal of Climatology*, *26*(3), 283–301. https://doi.org/10.1002/joc.1255

Kornhuber, K., Petoukhov, V., Petri, S., Rahmstorf, S., & Coumou, D. (2017). Evidence for wave resonance as a key mechanism for generating high-amplitude quasi-stationary waves in boreal summer. *Climate Dynamics*, *49*(5–6), 1961–1979. https://doi.org/10.1007/s00382-016-3399-6

Luo, D., Luo, B., & Zhang, W. (2023). A perspective on the evolution of atmospheric blocking theories: From eddy-mean flow interaction to nonlinear multiscale interaction. *Advances in Atmospheric Sciences*, *40*(4), 553–569. https://doi.org/10.1007/s00376-022-2194-z

Maddison, J. W., Gray, S. L., Martínez-Alvarado, O., & Williams, K. D. (2019). Upstream cyclone influence on the predictability of block onsets over the Euro-Atlantic region. *Monthly Weather Review*, *147*(4), 1277–1296. https://doi.org/10.1175/MWR-D-18-0226.1

Manola, I., Selten, F., de Vries, H., & Hazeleger, W. (2013). "Waveguidability" of idealized jets. *Journal of Geophysical Research: Atmospheres*, *118*(18), 10432–10440. https://doi.org/10.1002/jgrd.50758

Martin, J. E. (2021). Recent trends in the waviness of the Northern Hemisphere wintertime polar and subtropical jets. *Journal of Geophysical Research: Atmospheres*, *126*(9). https://doi.org/10.1029/2020JD033668

Martius, O., Schwierz, C., & Davies, H. C. (2006). A refined Hovmöller diagram. *Tellus A: Dynamic Meteorology and Oceanography*, *58*(2), 221–226. https://doi.org/10.1111/j.1600-0870.2006.00172.x

Martius, O., Schwierz, C., & Davies, H. C. (2010). Tropopause-level waveguides. *Journal of the Atmospheric Sciences*, *67*(3), 866–879. https://doi.org/10.1175/2009JAS2995.1

Masato, G., Hoskins, B. J., & Woollings, T. J. (2012). Wave-breaking characteristics of midlatitude blocking. *Quarterly Journal of the Royal Meteorological Society*, *138*(666), 1285–1296. https://doi.org/10.1002/qj.990

Massacand, A. C., & Davies, H. C. (2001). Interannual variability of the extratropical northern hemisphere and the potential vorticity wave guide. *Atmospheric Science Letters*, *2*(1–4), 61–71. https://doi.org/10.1006/asle.2001.0036

Methven, J., & Berrisford, P. (2015). The slowly evolving background state of the atmosphere. *Quarterly Journal of the Royal Meteorological Society*, *141*(691), 2237–2258. https://doi.org/10.1002/qj.2518

Nakamura, H., Nakamura, M., & Anderson, J. L. (1997). The role of high- and low-frequency dynamics in blocking formation. *Monthly Weather Review*, *125*(9), 2074–2093. https://doi.org/10.1175/1520-0493(1997)125⟨2074:TROHAL⟩2.0.CO;2

Nakamura, N., & Huang, C. S. Y. (2018). Atmospheric blocking as a traffic jam in the jet stream. *Science*, *361*(6397), 42–47. https://doi.org/10.1126/science.aat0721

Nakamura, N., & Solomon, A. (2011). Finite-amplitude wave activity and mean flow adjustments in the atmospheric general circulation. Part II: Analysis in the isentropic coordinate. *Journal of the Atmospheric Sciences*, *68*(11), 2783–2799. https://doi.org/10.1175/2011JAS3685.1

Nakamura, N., & Zhu, D. (2010). Finite-amplitude wave activity and diffusive flux of potential vorticity in eddy–mean flow interaction. *Journal of the Atmospheric Sciences*, *67*(9), 2701–2716. https://doi.org/10.1175/2010JAS3432.1

Nathan, T. R., & Hodyss, D. (2010). Troposphere-stratosphere communication through local vertical waveguides. *Quarterly Journal of the Royal Meteorological Society*, *136*(646), 12–19. https://doi.org/10.1002/qj.532

Petoukhov, V., Rahmstorf, S., Petri, S., & Schellnhuber, H. J. (2013). Quasiresonant amplification of planetary waves and recent Northern Hemisphere weather extremes. *Proceedings of the National Academy of Sciences*, *110*(14), 5336–5341. https://doi.org/10.1073/pnas.1222000110

Pfahl, S., Schwierz, C., Croci-Maspoli, M., Grams, C. M., & Wernli, H. (2015). Importance of latent heat release in ascending air streams for atmospheric blocking. *Nature Geoscience*, *8*(8), 610–614. https://doi.org/10.1038/ngeo2487

Polster, C. (2023). wavestoweather/Rolling-Zonalization: v1.1 [Software]. Zenodo. https://doi.org/10.5281/zenodo.10149381

Polster, C., & Wirth, V. (2023). The onset of a blocking event as a "traffic jam": Characterization with ensemble sensitivity analysis. *Journal of the Atmospheric Sciences*, *80*(7), 1681–1699. https://doi.org/10.1175/JAS-D-21-0312.1

Riboldi, J., Rousi, E., D'Andrea, F., Rivière, G., & Lott, F. (2022). Circumglobal Rossby wave patterns during boreal winter highlighted by space–time spectral analysis. *Weather and Climate Dynamics*, *3*(2), 449–469. https://doi.org/10.5194/wcd-3-449-2022

Röthlisberger, M., Martius, O., & Wernli, H. (2016). An algorithm for identifying the initiation of synoptic-scale Rossby waves on potential vorticity waveguides: Initiation of Rossby Waves on PV Waveguides. *Quarterly Journal of the Royal Meteorological Society*, *142*(695), 889–900. https://doi.org/10.1002/qj.2690

Rousi, E., Kornhuber, K., Beobide-Arsuaga, G., Luo, F., & Coumou, D. (2022). Accelerated western European heatwave trends linked to more-persistent double jets over Eurasia. *Nature Communications*, *13*(1), 3851. https://doi.org/10.1038/s41467-022-31432-y

Schwierz, C., Dirren, S., & Davies, H. C. (2004). Forced waves on a zonally aligned jet stream. *Journal of the Atmospheric Sciences*, *61*(1), 73–87. https://doi.org/10.1175/1520-0469(2004)061⟨0073:FWOAZA⟩2.0.CO;2

Spensberger, C., Spengler, T., & Li, C. (2017). Upper-tropospheric jet Axis detection and application to the boreal winter 2013/14. *Monthly Weather Review*, *145*(6), 2363–2374. https://doi.org/10.1175/MWR-D-16-0467.1

Steinfeld, D., Boettcher, M., Forbes, R., & Pfahl, S. (2020). The sensitivity of atmospheric blocking to upstream latent heating—Numerical experiments. *Weather and Climate Dynamics*, *1*(2), 405–426. https://doi.org/10.5194/wcd-1-405-2020

Teng, H., & Branstator, G. (2019). Amplification of waveguide teleconnections in the boreal summer. *Current Climate Change Reports*, *5*(4), 421–432. https://doi.org/10.1007/s40641-019-00150-x

White, R. H. (2019). Detecting waveguides for atmospheric planetary waves: Connections to extreme weather events. In C. Chen, A. Charantonis, J. Runge, & J. Brajard (Eds.), *Proceedings of the 9th international workshop on climate informatics: CI2019 9 (No. NCAR/TN- 561+PROC)* (pp. 219–223). UCAR/NCAR. https://doi.org/10.5065/Y82J-F154

White, R. H., Kornhuber, K., Martius, O., & Wirth, V. (2022). From atmospheric waves to heatwaves: A waveguide perspective for understanding and predicting concurrent, persistent, and extreme extratropical weather. *Bulletin of the American Meteorological Society*, *103*(3), E923–E935. https://doi.org/10.1175/BAMS-D-21-0170.1

Wirth, V. (2020). Waveguidability of idealized midlatitude jets and the limitations of ray tracing theory. *Weather and Climate Dynamics*, *1*(1), 111–125. https://doi.org/10.5194/wcd-1-111-2020

Wirth, V., & Polster, C. (2021). The problem of diagnosing jet waveguidability in the presence of large-amplitude eddies. *Journal of the Atmospheric Sciences*, *78*(10), 3137–3151. https://doi.org/10.1175/JAS-D-20-0292.1

Wirth, V., Riemer, M., Chang, E. K. M., & Martius, O. (2018). Rossby wave packets on the midlatitude waveguide—A review. *Monthly Weather Review*, *146*(7), 1965–2001. https://doi.org/10.1175/MWR-D-16-0483.1